Chemical Science

ROYAL SOCIETY OF CHEMISTRY

EDGE ARTICLE

View Article Online
View Journal | View Issue

Cite this: *Chem. Sci.*, 2024, **15**, 3485

All publication charges for this article have been paid for by the Royal Society of Chemistry

Iron(IV) alkyl complexes: electronic structure contributions to Fe–C bond homolysis and migration reactions that form N–C bonds from N_2†

Samuel M. Bhutto, Reagan X. Hooper, Sean F. McWilliams, Brandon Q. Mercado and Patrick L. Holland *

High-valent iron alkyl complexes are rare, as they are prone to Fe–C bond homolysis. Here, we describe an unusual way to access formally iron(IV) alkyl complexes through double silylation of iron(I) alkyl dinitrogen complexes to form an $NNSi_2$ group. Spectroscopically validated computations show that the disilylehydrazido(2−) ligand stabilizes the formal iron(IV) oxidation state through a strongly covalent Fe–N π-interaction, in which one π-bond fits an "inverted field" description. This means that the two bonding electrons are localized more on the metal than the ligand, and thus an iron(II) resonance structure is a significant contributor, similar to the previously-reported phenyl analogue. However, in contrast to the phenyl complex which has an $S = 1$ ground state, the ground state of the alkyl complex is $S = 2$, which places one electron in the π* orbital, leading to longer and weaker Fe–N bonds. The reactivity of these hydrazido(2−) complexes is dependent on the steric and electronic properties of the specific alkyl group. When the alkyl group is the bulky trimethylsilylmethyl, the formally iron(IV) species is stable at room temperature and no migration of the alkyl ligand is observed. However, the analogous complex with the smaller methyl ligand does indeed undergo migration of the carbon-based ligand to the $NNSi_2$ group to form a new N–C bond. This migration is followed by isomerization of the hydrazido ligand, and the product exists as two isomers that have distinct η^1 and η^2 binding of the hydrazido group. Lastly, when the alkyl group is benzyl, the Fe–C bond homolyzes to give a three-coordinate hydrazido(2−) complex which is likely due to the greater stability of a benzyl radical compared to that for methyl or trimethylsilylmethyl. These studies demonstrate the availability of a hydrocarbyl migration pathway at formally iron(IV) centers to form new N–C bonds directly to N_2, though product selectivity is highly dependent on the identity of the migrating group.

Received 6th November 2023
Accepted 16th January 2024

DOI: 10.1039/d3sc05939a

rsc.li/chemical-science

Introduction

The isolation of iron(IV) compounds has been dominated by oxo, nitrido, and imido complexes, because the π-bonds in these compounds help to stabilize this high oxidation state.[1–13] In contrast, reports of organometallic iron(IV) alkyl complexes are rare.[14–19] One reason for this trend is that high-valent iron alkyl species are prone to Fe–C bond homolysis to produce alkyl radicals,[15,17] exemplified by the well-documented reactivity of alkyliron porphyrin and corrole complexes (Fig. 1a).[20–26] In contrast, Wolczanski and coworkers reported NHC-supported alkyliron(IV) complexes that were more resistant to Fe–C homolysis, and instead underwent alkyl group migration to the imido ligand to produce the corresponding amidoiron(II) complexes (Fig. 1b).[16] To our knowledge, this is the only well-characterized example of alkyl migration from a transition metal to a M=NR group, though a migration step may be involved in some reactions where a metal-alkyl undergoes amination by addition of an azide.[27,28] Meyer has also reported insertion of a coordinated NHC ligand into the Co–N bond of a Co=NR complex,[29] and there are several reports of carbenes inserting into Fe–N single bonds associated with supporting ligands.[29–33]

Our research in this area emerged from the study of formally iron(IV) aryl species that undergo migration of the aryl group to the Fe-bound NNR_2 group (Scheme 1).[34–36] The reaction sequence of interest starts with the reaction of iron(I) aryl N_2 complexes (**1-N$_2$**) with two equivalents of Me_3SiX (X = Br, I, OTf; OTf = trifluoromethanesulfonate) and one equivalent of reducing agent. This gives a double silylation at the distal N atom and net three-electron oxidation at the metal, resulting in a formally iron(IV) complex with aryl and hydrazido(2−) ligands (**2**). It is this complex that can perform the migration of the aryl

Department of Chemistry, Yale University, New Haven, Connecticut 06520, USA. E-mail: patrick.holland@yale.edu

† Electronic supplementary information (ESI) available: Details on experimental methods, spectroscopy, crystallography, and computations. CCDC 2226338–2226342, 2226344, and 2303073. For ESI and crystallographic data in CIF or other electronic format see DOI: https://doi.org/10.1039/d3sc05939a

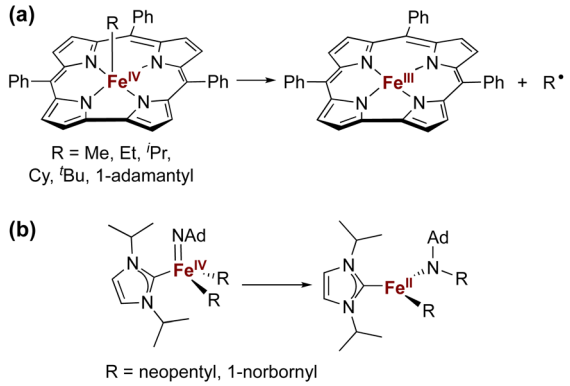

Fig. 1 Examples of previously reported iron(IV) alkyl complexes and degradation pathways.

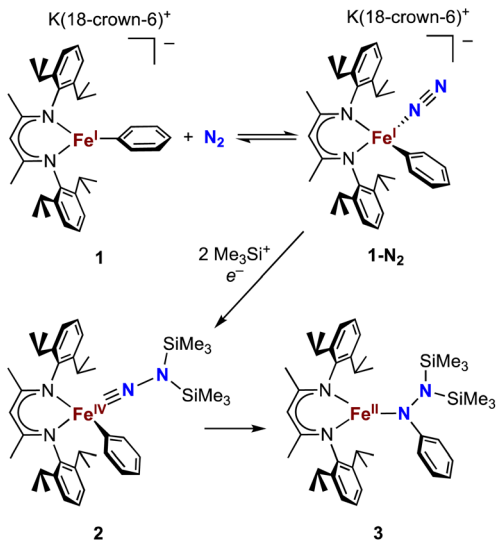

Scheme 1 Formation of a formally iron(IV) hydrazido(2−) complex from N_2, and subsequent migratory insertion of the aryl ligand.

group from Fe to the proximal N atom to form a new N–C bond in a hydrazido product (**3**).

So far, the migrations of hydrocarbyl groups from Fe to a multiply-bound N ligand that we have reported have been limited to iron–aryl complexes.[35,36] Since N_2 binding has been reported in a β-diketiminatoiron(I) alkyl complex as well,[37] we hypothesized that iron(IV) alkyl hydrazido(2−) complexes might undergo alkyl migration by analogy to the aryl migrations. Previously, Peters described hydride migration to a hydrazido(2−) ligand at a formally iron(IV) center, suggesting that migration chemistry is not limited to aryl groups.[38] However, we found that alkynyl groups do not migrate in the diketiminate system.[36] Here, we describe a series of iron(I) alkyl complexes that bind N_2 at low temperatures and their reactivities upon N_2 silylation, including the characterization of the first formally iron(IV) alkyl hydrazido(2−) complex that is stable at room temperature. In some cases, N–C bond formation occurs but in other cases homolysis causes loss of the alkyl group without N–C bond formation, and the differences give insight into the feasibility of iron(IV) in these different environments. Density functional theory (DFT) calculations elucidate the competition between Fe–C homolysis and alkyl migration pathways. A preliminary description of this research has been shared in a preprint.[39]

Results and discussion

Binding of N_2 to iron(I) alkyl complexes

The alkyl chemistry described here starts from the known high-spin three-coordinate iron(II) alkyl complexes **4a–4c**.[37,40–42] Previous work has shown that an analogous β-diketiminatoiron(II) alkyl complex can be reduced to an iron(I) complex, which upon cooling can bind N_2 at the iron center.[34,37] Accordingly, we prepared the iron(I) complexes **5a–5c** by reduction of the corresponding iron(II) alkyl complexes with KC_8 in the presence of 18-crown-6, and isolated them in *ca.* 80% yield (Scheme 2). Complex **5c** was isolated and fully characterized previously.[37] Crystals of the new complexes **5a** and **5b**, grown from THF/hexanes, yielded X-ray crystallographic structures (Fig. 2). The average Fe–N bond lengths of **5a** (1.928(5) Å) and **5b** (1.918(3) Å) are equivalent to the distance in **5c** (1.922(4) Å). The Fe–C bond length of **5b** (2.063(4) Å) is longer than that in the starting iron(II) complex **4b** (2.041(2) Å),[42] consistent with the lower oxidation state, while the Fe–C bond lengths of **5a** and **4a** are indistinguishable (**5a**, avg. 2.015(2) Å; **4a**, 2.022(2) Å).[42] The Mössbauer parameters of **5a** ($\delta = 0.44$ mm s^{-1}, $|\Delta E_Q| = 1.90$ mm s^{-1}) and **5b** ($\delta = 0.27$ mm s^{-1}, $|\Delta E_Q| = 1.75$ mm s^{-1}) are similar to those reported for high-spin **5c** ($\delta = 0.38$ mm s^{-1}, $|\Delta E_Q| = 2.06$ mm s^{-1}).[43] Consistent with this assignment, solution magnetic susceptibilities indicate high-spin ($S = 3/2$) ground states for **5a** ($\mu_{eff} = 4.3(1)\ \mu_B$) and **5b** ($\mu_{eff} = 4.3(1)\ \mu_B$).

We then tested N_2 binding at the iron(I) alkyl complexes at low temperature. Freezing solutions of **5a–5c** in THF under an atmosphere of N_2 led to a color change of the solutions from green to magenta, and thawing the solutions gave back the original green color. These color changes were not observed when freezing solutions under an atmosphere of Ar. van't Hoff analysis of the variable-temperature ^{1}H NMR (**5a** and **5b**) and

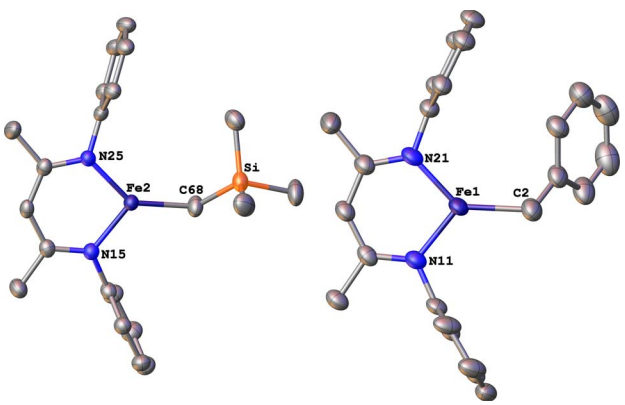

Fig. 2 ORTEP diagrams of the iron(I) complexes **5a** (left) and **5b** (right) with thermal ellipsoids shown at 50% probability. H atoms, iPr groups, and K(18-crown-6)(THF)$_2^+$ cations are omitted for clarity, as well as a molecule of THF in the asymmetric unit of **5a**.

Table 1 Results from van't Hoff analysis of variable-temperature spectroscopic measurements of **5a–5c** under N_2

	Alkyl group	ΔH (kcal mol^{-1})	ΔS (e.u.)
5a	CH_2SiMe_3	−8.8(6)	−52(3)
5b	CH_2Ph	−9.5(6)	−57(2)
5c	CH_3	−4.3(7)	−33(3)

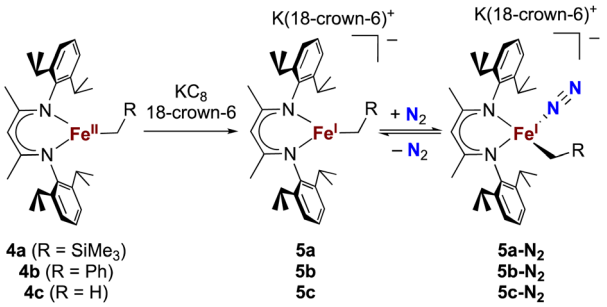

Scheme 2 Synthesis of iron(I) alkyl complexes **5a–5c** and reversible N_2 binding.

UV-vis (**5c**) spectra gave the thermodynamic parameters shown in Table 1. The negative enthalpy and entropy values for each complex are consistent with N_2 binding at lower temperatures, likely in an end-on fashion as proposed in the analogous iron β-diketiminate systems mentioned above.[34–37]

Silylation of N_2 in the trimethylsilylmethyliron complex leads to an isolable iron(IV) alkyl complex

Next we explored the silylation reactions of the N_2-bound iron(I) complexes to form formally iron(IV) complexes (Scheme 3). Addition of the bis(silyl) reagent **6** to a mixture of **5a-N$_2$** and K(18-crown-6)($C_{10}H_8$) (used as an external reductant) in Et_2O at −116 °C led to an immediate color change from magenta to brown. The ^{1}H NMR spectrum of the crude reaction mixture showed the formation of a new C_s symmetric complex in 73% spectroscopic yield. Cooling a concentrated hexamethyldisiloxane (HMDSO) solution at −35 °C overnight led to the isolation of brown crystals in 32% yield, which were identified by X-ray diffraction as the formally iron(IV) complex **7a** (Fig. 3, top). The N–N bond length is 1.326(3) Å, which lies between the values for

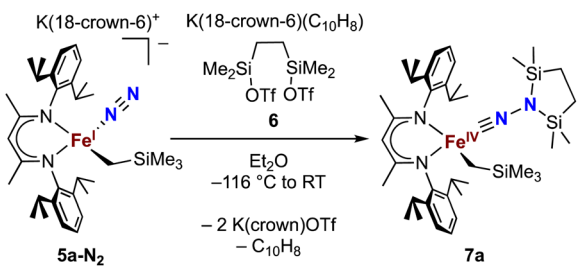

Scheme 3 Synthesis of the formally iron(IV) complex **7a**.

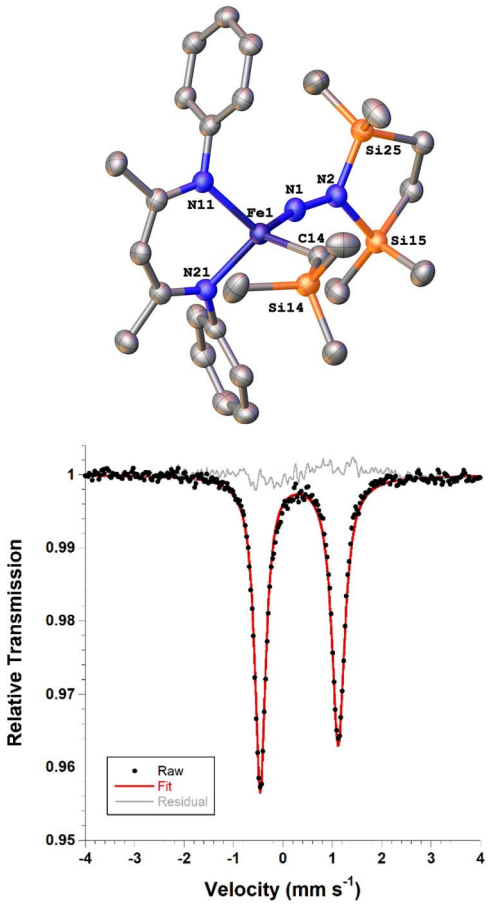

Fig. 3 (Top) ORTEP diagram of **7a** with thermal ellipsoids shown at 50% probability, with H atoms and ^{i}Pr groups omitted for clarity. (Bottom) Solid state zero-field Mössbauer spectrum of **7a** at 80 K. The black circles are the data, the red line is the fit, and the grey line is the residual (data − fit).

a N–N single bond (1.45 Å) and double bond (1.25 Å) in the corresponding organic N_2H_x compounds, and is comparable to those in other four-coordinate iron hydrazido(2−) complexes as well as the phenyl complex **2** (1.340(4) Å).[35,44,45] However, the bond lengths to iron in **7a** are significantly different than those in **2**. The Fe–N_{hyd} bond length (1.749(2) Å) and average Fe–N_{nacnac} bond length (2.051(1) Å) in **7a** are ∼0.08 Å longer than those in **2** (1.673(3) and 1.970(2) Å, respectively). Additionally, the iron center in **7a** adopts a distorted tetrahedral geometry ($\tau_4 = 0.88$) rather than the distorted trigonal pyramidal geometry in **2** ($\tau_4 = 0.75$).

The zero-field Mössbauer spectrum of **7a** consists of a doublet with an isomer shift of $\delta = 0.33$ mm s^{-1}, which is much higher than the value of $\delta = 0.17$ mm s^{-1} in **2** (Fig. 3, bottom). The higher isomer shift in **7a** may indicate that the complex has a different ground spin state, and the longer bonds in **7a** noted above suggest the higher spin state of $S = 2$. Furthermore, the bond distances to the iron center in **7a** closely resemble those observed in a DFT model of **2** in an $S = 2$ state (see ESI†).[35] Finally, a solution magnetic susceptibility measurement gave $\mu_{eff} = 5.0(2)\ \mu_B$, which confirms the high-spin ground state.

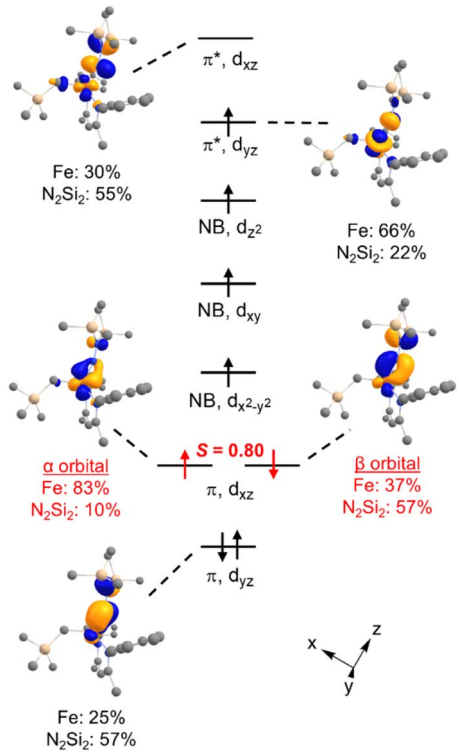

Fig. 4 Qualitative molecular orbital diagram showing the QROs of **7a** ($S = 2$) with selected QRO plots shown at an isovalue of 0.05 au. In red are the one-electron orbitals for the "corresponding pair" of electrons in the spin-polarized Fe–N π-bond.

Electronic structure of the alkyl hydrazido(2−) complex

DFT calculations were performed for greater insight into the electronic structure of **7a**. The geometry of **7a** in an $S = 2$ ground state was optimized at the B3LYP/def2-TZVP level, giving bond metrics that agree with those in the experimental X-ray structure of **7a** (see ESI for details†). This computational model was further validated by computing[46] the expected Mössbauer parameters of $\delta = 0.37$ mm s^{-1} and $|\Delta E_Q| = 1.63$ mm s^{-1}, which are close to the experimental values of 0.33 and 1.58 mm s^{-1}, respectively. The quasi-restricted orbitals (QROs) from the model of **7a** are shown in Fig. 4, with the z axis along the Fe–hydrazido(2−) bond. The formal bond order of the Fe–N_{hyd} bond is 2.5, as the Fe d_{yz} π* orbital is singly occupied. This is consistent with the longer Fe–N_{hyd} bond distance in **7a** compared with that of **2**, which has an $S = 1$ ground state and a formal Fe–N_{hyd} bond order of 3.

The Fe–N_{hyd} π bonding interaction involving the Fe d_{yz} orbital has more hydrazido than iron character, typical of a normal π bond. The π bonding interaction involving the Fe d_{xz} orbital, however, is more complex. The doubly-occupied Fe–N_{hyd} π bonding orbital has a relatively low orbital overlap of $\langle\alpha|\beta\rangle = 0.80$, and thus it is spin-polarized with the α electron lying 83% on the Fe and the β electron lying only 37% on Fe. Additionally, the unoccupied Fe–N_{hyd} π* orbital has significantly less Fe character than N_2Si_2 ligand character, indicative of an "inverted ligand field."[47,48] Taken together, the large spin polarization of one of the Fe–N_{hyd} π bonding orbitals and "inverted" ligand character suggests that the formally hydrazido(2−) ligand may be alternatively described as a neutral NNR_2 (isodiazene) implying an iron(II) oxidation state. This situation is analogous to that described for the metastable formally iron(IV) phenyl complex **2**,[35] with one spin-polarized orbital having Fe–N π character.

From the available data, it is difficult to discern why **7a** has a different ground spin state than **2**, as the energetic differences between the two are small. It is possible that the somewhat lower relative energy of the $S = 2$ state in **7a** arises because the geometry is distorted from trigonal pyramidal toward tetrahedral, leading to a weaker ligand field.

To further probe the redox noninnocence of the NNR_2 ligand in **7a**, multireference CASSCF(8,7) calculations were performed on the DFT-optimized $S = 2$ structure; details are shown in the SI. The dominant configuration (72%) has the expected Hund filling, corresponding to a hydrazido(2−) ligand. The next two most important configurations have single (16%) and double (10%) occupation of the Fe–N π antibonding orbital involving the Fe d_{xz} orbital, which correspond to iron(III) hydrazido and iron(II) isodiazene descriptions of **7a**, respectively. Thus, both single reference and multireference calculations point to ligand noninnocence of the NNR_2 ligand, to an extent that is comparable to the phenyl and alkynyl analogues.[35,36]

The trimethylsilylmethyl group does not migrate

We then turned to the solution behavior of **7a**. Complex **7a** was much more stable in solution than **2**, showing only about 25% decomposition after 4 days in C_6D_6 solution at room temperature (whereas **2** is completely consumed within a few hours at room temperature). Heating a C_6D_6 solution of **7a** at 80 °C for 2 hours led to its complete consumption. However, the product was not alkyl migration (in analogy to **2**) but rather formation of the iron(II) alkyl complex **4a** (24%), the hydrazido(2−) product **8** (29%), and the amido complex LFeN($Me_2Si(CH_2)_2SiMe_2$) (36%) (see ESI for details†). By analogy to a related N–Si bond cleavage in an iron silyldiazenido complex by Ashley,[49] we speculate that the mechanism for the formation of **4a** might involve homolytic cleavage of N–Si bonds, though there is also cleavage of Fe–C, Fe–N, and N–N bonds to yield the other observed products.

Why does the trimethylsilylmethyl group in **7a** not migrate as previously observed for the phenyl group in **2**? Though it is tempting to attribute this to the difference in the spin state, we were not able to optimize transition states for migration of the CH_2SiMe_3 group (triplet or quintet states) to assess the impact of spin state and TS geometry with DFT. However, since the electronically similar methyl group does migrate (see below), there is some evidence that steric effects play a role.

Attempts to generate the iron(IV)-benzyl lead to homolysis

We also explored the N_2 silylation reactivity of the other iron(I) alkyl complexes. In contrast with the silylation of **5a-N_2**, the use of K(18-crown-6)($C_{10}H_8$) as an external reductant in the reaction of the iron(I) benzyl complex **5b-N_2** and the silyl triflate **6** led to an intractable mixture of unidentified species. However, it has

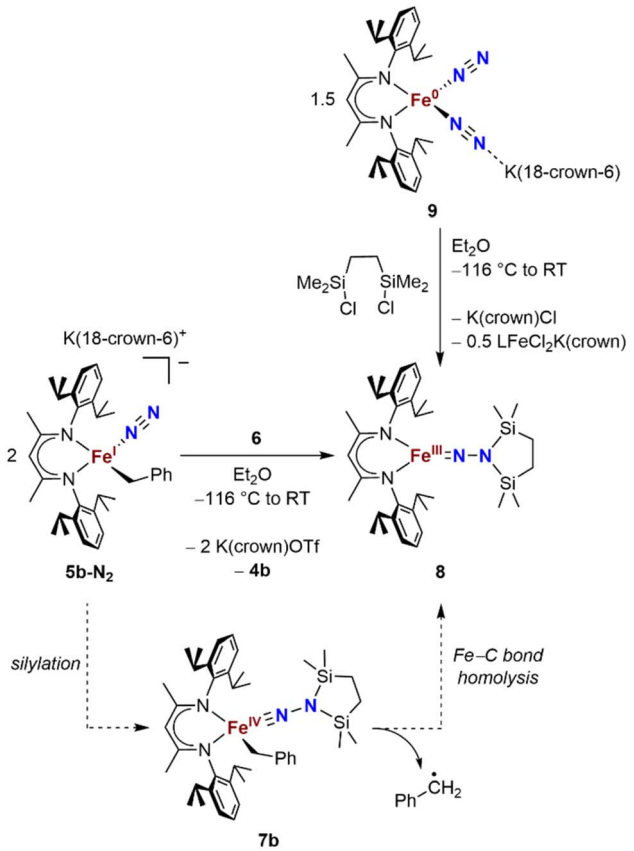

Scheme 4 Syntheses of the iron(III) hydrazido(2−) complex **8**, and proposed mechanism of formation from **5b-N$_2$**.

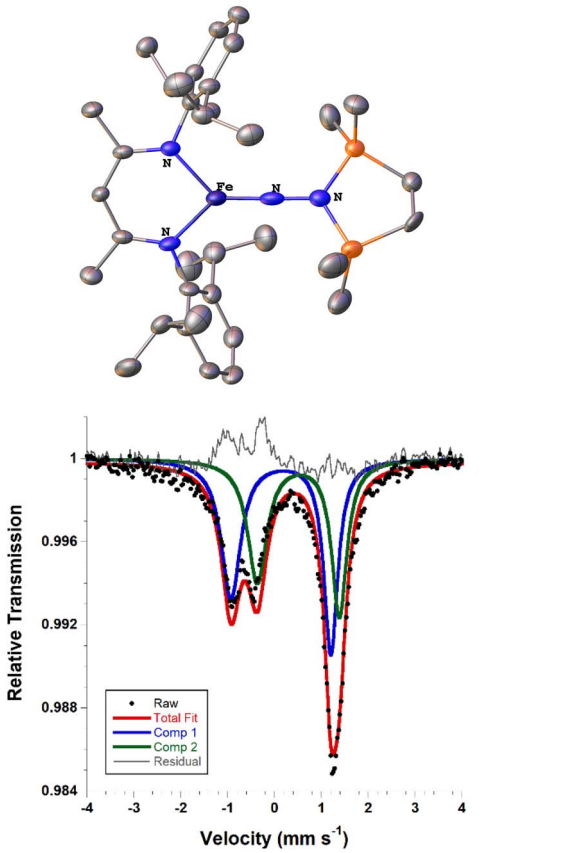

Fig. 5 (Top) ORTEP diagram of **8** with thermal ellipsoids shown at 50% probability and H atoms omitted for clarity; due to apparent disorder in the core, the structure is for connectivity only. (Bottom) Solid state zero-field Mössbauer spectrum of **8** at 80 K. The black circles are the data, the blue and green lines are the components of the fit, the red line is the sum of the components, and the grey line is the residual (data – fit).

previously been shown in the synthesis of a related aryl diazenido species that the starting iron(I) aryl complex can provide the necessary electron equivalent in the reaction (unfortunately limiting the yield of silylated product to a maximum of 50% based on iron, since part of it is a sacrificial reductant).[34] Thus, addition of **6** to a solution of **5b-N$_2$** in Et$_2$O at −116 °C without an external reductant led to the formation of the oxidized iron(II) product **4b** in 64% spectroscopic yield (yield based on the stoichiometry in Scheme 4, quantified by ^{1}H NMR spectroscopy), as well as a new C_{2v} symmetric species **8** in 22% spectroscopic yield (Scheme 4, middle). This same species **8** was also identified in the decomposition mixture of **7a** in 27% spectroscopic yield, indicating that it had lost the alkyl group. Indeed, X-ray diffraction revealed **8** to be an iron(III) hydrazido(2−) complex (Fig. 5, top).

Compound **8** is closely related to an iron(III) hydrazido(2−) complex we previously reported, the trimethylsilyl analogue LFeNN(SiMe$_3$)$_2$ (L = 2,4-bis(2,6-diisopropylphenylimido)pentyl).[50] Accordingly, complex **8** could be prepared independently from the reaction of the iron(0)-bis(dinitrogen) complex **9** and 1,2-bis(chlorodimethylsilyl)ethane in 22% isolated yield (Scheme 4, upper right). The products from the two synthetic methods had identical ^{1}H NMR spectra, further supporting the proposed composition of **8**.

We propose that the route from **5b-N$_2$** to **8** begins with silylation to give the formally iron(IV) complex **7b** followed by Fe–C bond homolysis,[17,26,51,52] producing a benzyl radical (Scheme 4, bottom). In order to test this idea, we performed trapping experiments using the radical scavenger TEMPO (TEMPO = 2,2,6,6-tetramethylpiperidine 1-oxyl). When TEMPO was added to the reaction mixture immediately after silane addition at −116 °C, ^{1}H NMR spectroscopy showed >80% formation of TEMPO-Bn.[53] This implies the formation of a transient intermediate that can release benzyl radicals.

Unfortunately, the X-ray crystal structure solution of **8** had a second component in the core, and the disorder prevents us from deriving reliable metrical parameters, and we were unable to obtain satisfactory results from CHN analysis. Despite these problems that prevent deep study of **8**, we note in passing several intriguing aspects of its spectroscopic properties. Similar to the previously characterized trimethylsilyl analogue LFeNN(SiMe$_3$)$_2$,[50] the solid state Mössbauer spectrum of crystalline **8** collected at 80 K shows two doublets in a 1 : 1 ratio with isomer shifts of 0.13 and 0.51 mm s^{-1} (Fig. 5, bottom). In the previous work, the 1 : 1 ratio was explained by the presence of

Table 2 Comparison of Mössbauer parameters between experiment and DFT models (BP86/def2-TZVP or B3LYP/def2-TZVP)

Compound	Functional	Spin state	Rel. energy (kcal mol^{-1})	δ (mm s^{-1})	$\lvert\Delta E_Q\rvert$ (mm s^{-1})
8	Exp.	1/2		0.13	2.13
		3/2		0.51	1.75
	BP86	1/2	0	0.12	2.04
		3/2	9	0.48	1.83
	B3LYP	1/2	2	0.24	1.76
		3/2	0	0.67	1.36
LFeNN(SiMe$_3$)$_2$ (ref. 55)	Exp.	1/2		0.22	1.99
		3/2		0.46	1.16
	BP86	1/2	0	0.14	1.93
		3/2	9	0.51	1.72
		5/2	31	0.61	3.69
	B3LYP	1/2	1		
		3/2	0		
		5/2	15		

two molecules with significantly different bond distances, which coexist in alternating positions in the crystals. Comparison to calculations and fitting of magnetic susceptibility data supported our conclusion that the two molecules had different spin states ($S = 1/2$ and $S = 3/2$).[50] In order to determine whether this might be the case in **8** as well, DFT calculations were carried out to determine the relative energies of the $S = 1/2$ and $S = 3/2$ states using geometry-optimized structures of **8** (Table 2). Calculations using both the BP86 and B3LYP functionals show a small energy difference between the doublet and quartet states: using BP86 the low-spin conformer is lower in energy by 9 kcal mol^{-1}, while B3LYP predicts the high-spin state to be lower in energy by 2 kcal mol^{-1}. This difference in lowest energy calculated spin conformer is not surprising, as hybrid functionals such as B3LYP have been shown to favor higher spin states.[54] These small calculated differences in energy suggest that the actual spin isomers could indeed be isoenergetic. Importantly, the calculated Mössbauer parameters of the geometry-optimized doublet and quartet DFT models are in excellent agreement with the two signals in the spectrum of **8** (Table 2).[46]

Additionally, the electron paramagnetic resonance (EPR) spectrum of a frozen toluene solution of **8** collected at 5 K shows two overlapping signals consistent with coexisting $S = 1/2$ and $S = 3/2$ species (Fig. 6). Simulating the spectrum gives an $S = 1/2$ species with $g = [1.80, 1.84, 3.54]$. The large anisotropy of g values was similarly observed in the previously reported trimethylsilyl analogue which had $g = [1.79, 1.84, 3.61]$.[50] The small signals with g_{eff} values of 6.21 and 2.32 are reminiscent of a three-coordinate, intermediate-spin ($S = 3/2$) iron(III) imido complex with the same diketiminate supporting ligand,[55,56] supporting this assignment. Overall, it appears that spin isomerism is present in this three-coordinate iron(III) hydrazido(2−) complex. Future studies will aim to unravel the reason why the 1 : 1 ratio is observed even without apparent crystal constraints.

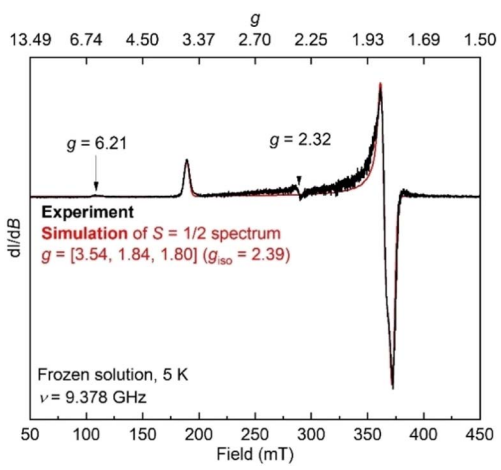

Fig. 6 EPR spectrum of **8** in toluene at 5 K (black) and simulation of the $S = 1/2$ component (red).

Methyl migration followed by silyl migration leads to a different kind of complex, with spin and coordination isomers

Finally, we explored the silylation of the iron(I) methyl complex **5c** (Scheme 5). Addition of the disilyl electrophile **6** to a solution of **5c-N$_2$** in Et$_2$O at −116 °C led to an immediate color change from magenta to brown, and then the mixture turned yellow upon warming to ambient temperature. The ^{1}H NMR spectrum of the crude reaction mixture showed the presence of two species: the oxidized iron(II) complex **4c** (57%) and a new C_s symmetric species **10** (37%). In this case, no formation of **8** (which would result from loss of a methyl radical) was observed in the crude mixture. X-ray crystallography identified **10** as a 1,2-bis(silyl)methylhydrazido complex (Fig. 7), with disorder that indicates co-crystallization of η^1 and η^2 isomers (described

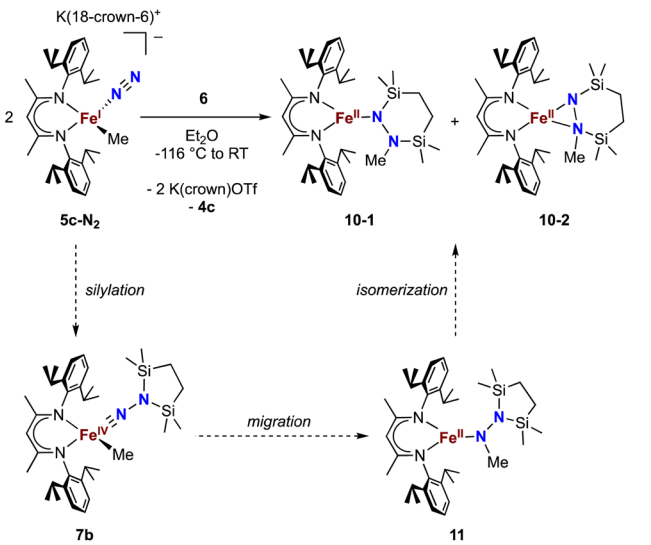

Scheme 5 Synthesis of the methylhydrazido complex **10**, which crystallizes as two isomers **10-1** and **10-2**. Along the bottom is shown the proposed mechanism of the reaction.

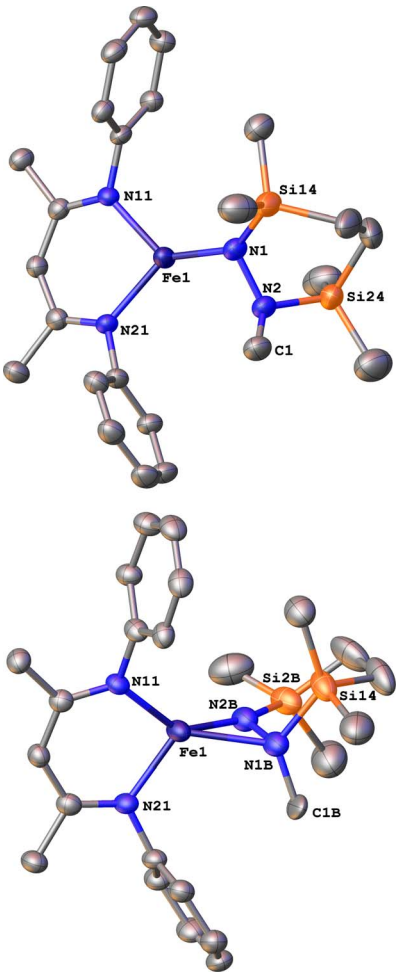

Fig. 7 ORTEP diagrams of **10-1** and **10-2** with thermal ellipsoids shown at 50% probability and H atoms and ^{i}Pr groups omitted for clarity. The η^1 isomer (major component **10-1**, 75%) is shown on the top, and the η^2 isomer (minor component **10-2**, 25%) is shown on the bottom.

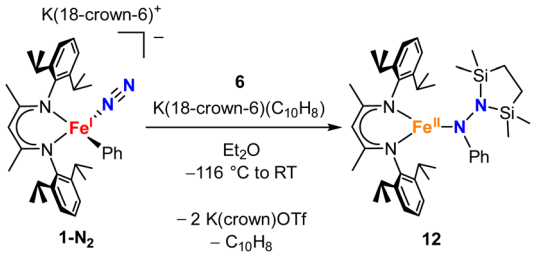

Scheme 6 Synthesis of the phenyl-migrated complex **12**.

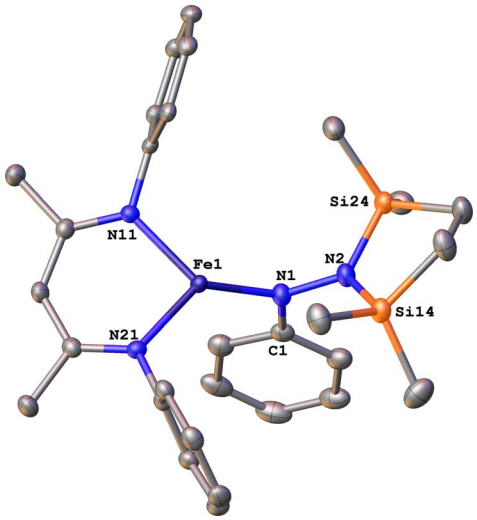

Fig. 8 ORTEP diagram of **12** with thermal ellipsoids shown at 50% probability. H atoms and ^{i}Pr groups omitted for clarity.

in more detail below). A reasonable mechanism for the formation of **10** is through the initial formation of the formally iron(IV) complex **7c**, followed by methyl migration to form the expected methylhydrazido complex **11** (Scheme 5, bottom). This complex could then isomerize through a silyl shift to give the observed product **10**. Shifting of the bis(silyl)methylhydrazido ligand in this way has precedent in the isomerization of free bis(trimethylsilyl)methylhydrazine, which can shift its silyl groups in the presence of catalytic amounts of base.[57] Most relevantly, Peters has reported an example of a disilylhydrazido(2−) complex in which the silyl group is proposed to go through an intermediate that resembles **10**.[58]

To test whether the ability of the silyl to shift arises somehow from the change from trimethylsilyl to the bis(silyl) reagent **6**, we prepared the bis(silyl) analogue of **2**. Specifically, the iron(I) phenyl complex **1-N_2** was treated with **6** in the presence of K(18-crown-6)($C_{10}H_8$) (Scheme 6),[34] which led to the expected 1,1-bis(silyl)phenylhydrazido complex **12** (Fig. 8) without the silyl shift observed in the methyl system. It is unclear whether the lack of isomerization by **12** to give the 1,2-bis(silyl)phenylhydrazido complex is the result of a high kinetic barrier or a thermodynamically unfavorable reaction. Regardless, this result suggests that the use of the bis(silyl) reagent is not the sole reason for hydrazido isomerization, and that the identity of the hydrocarbyl group on the hydrazido ligand influences its ability to take part in the silyl shift.

Isomers of compound 10

The X-ray crystal structure of **10** was disordered, and the best-fit model has two components, as mentioned above. Though both components contain the same cyclic ligand, its coordination to iron in one of the components (**10-1**) is η^1 (roughly 75% occupancy), whereas the other (**10-2**) is η^2 through both nitrogen atoms (roughly 25% occupancy). Accordingly, the Mössbauer spectrum of **10** has a shoulder that is indicative of multiple components, and the spectrum could be fit with two or three Mössbauer doublets (Fig. S21 and S22†). Because both X-ray and Mössbauer methods suggested multiple isomers in samples that were pure (as judged by CHN analysis), we explored the energies and geometries of both isomers in triplet and quintet states using DFT geometry optimizations (Table S10†). These indicated that there are three forms that have low energies (within 4 kcal mol^{-1} of one another): an η^1 isomer in a quintet

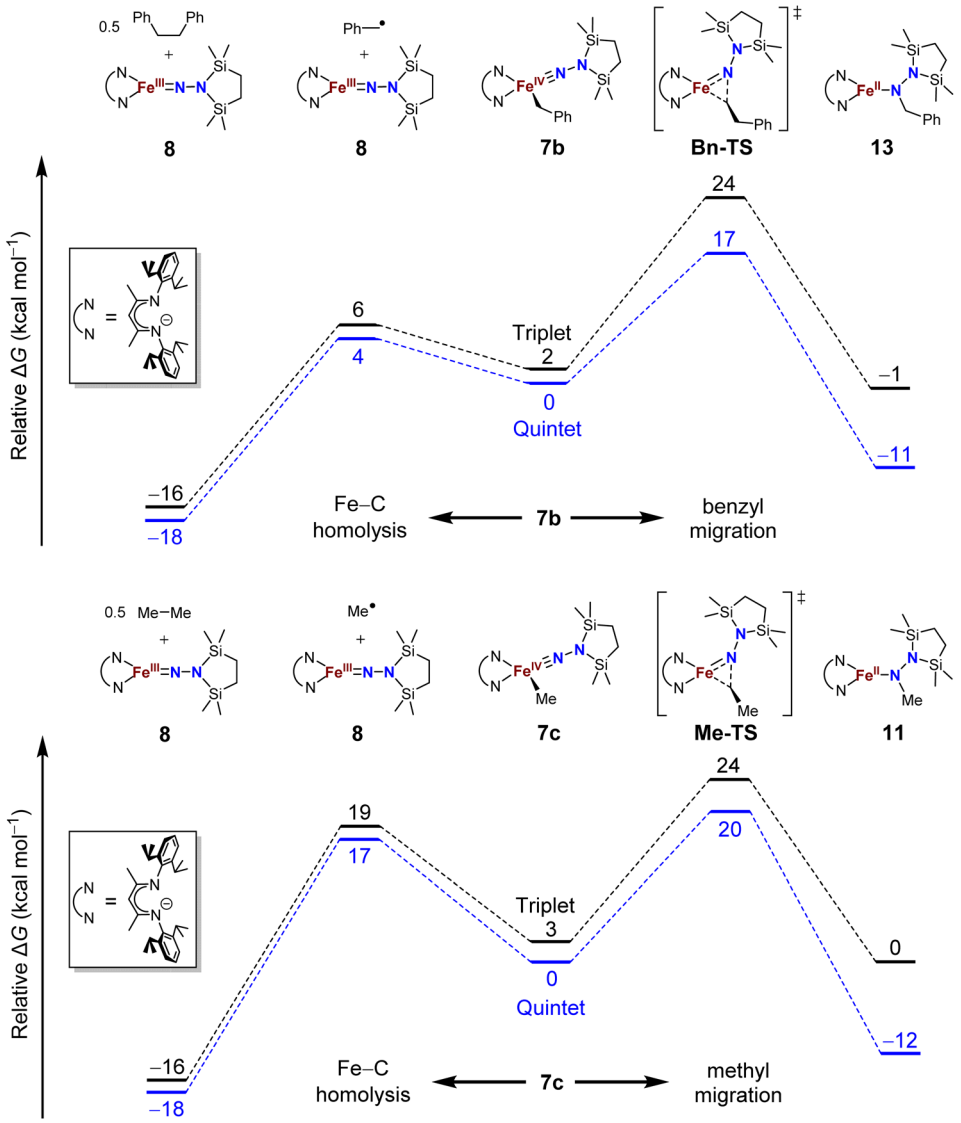

Fig. 9 Potential energy surfaces of Fe–C bond homolysis (to the left) *versus* alkyl migration (to the right) starting from the proposed iron(IV) benzyl (top) and methyl (bottom) complexes from DFT calculations (B3LYP/def2-TZVP).

state, and η^2 isomers in triplet or quintet states. Further, a superposition of signals with the calculated isomer shift and quadrupole splitting values from these three models fits well to the experimental Mössbauer spectrum (Table S11†). Finally, the predominance of quintet states agrees with the experimental solution magnetic moment of **10** of $\mu_{eff} = 5.1(2)\ \mu_B$. Though the limited amount of experimental information hinders our ability to delve further, this combination of spectroscopy, crystallography, and computations is consistent with the idea that multiple isomers could coexist and be distinct in the solid-state structure (though equilibrating on a subsecond timescale such that one set of resonances is observed by ^{1}H NMR spectroscopy).

DFT computations give insight into product selectivity

The difference in product speciation between the silylation reactions of the benzyl complex **5b** and the methyl complex **5c** suggests that there may be two competing reaction pathways upon formation of the resulting formally iron(IV) alkyl complexes: Fe–C homolysis and hydrocarbyl migration. These two competing reaction pathways were investigated using DFT calculations (Fig. 9, next page). Geometries were optimized using DFT (B3LYP/def2-TZVP) in both the triplet and quintet states to probe possible spin crossover as observed in the aryl migration mechanism.[35]

No transition states were found for the Fe–C_{alkyl} bond homolysis steps in either the benzyl (Fig. 9, top) or methyl (Fig. 9, bottom) system. This is not surprising, because bond homolysis reactions often have barriers very close to the BDFE if uncomplicated by steric constraints or spin state changes.[59] The quintet surface was calculated to be the lowest energy pathway for Fe–C homolysis in both systems. The products of Fe–benzyl bond homolysis are only 4 kcal mol^{-1} uphill from **7b**, while products of Fe–methyl homolysis are higher at 17 kcal mol^{-1}

relative to **7c**. This difference likely stems from the greater stability of a benzyl radical relative to a methyl radical.[60] Therefore, alkyl radical formation is expected to be much more rapid for the benzyl complex.

To assess the alkyl migrations, the nudged elastic band method was used to find transition states, which were then optimized. The lowest energy pathways for both benzyl and methyl migration were found on the quintet surfaces. The calculated barriers for benzyl (17 kcal mol^{-1}) and methyl (20 kcal mol^{-1}) migration are similar to the experimentally measured activation barriers for aryl migration reactions (21–23 kcal mol^{-1}).[35]

The significantly lower energy for Fe–C_{Bn} bond homolysis compared to the barrier for benzyl migration is consistent with the observation that silylation of **5b-N_2** gave homolysis to the iron(III) complex **8** rather than migration. Meanwhile, the energy for Fe–C_{Me} bond homolysis starting from **7c** is similar to the barrier for methyl migration, suggesting that after the silylation of **5c-N_2**, homolysis could potentially compete with the migration pathway. We cannot rule out the possibility that radical recombination after Fe–C_{Me} bond homolysis forms **11** in a two-step migration mechanism.[21]

Conclusions

In summary, the above studies have demonstrated that silylation of iron(I) alkyl N_2 complexes can give formally iron(IV) alkyl hydrazido(2−) species, with interesting differences in the subsequent reactivity. A methyl group does migrate, though it is followed by a silyl migration. With the bulkier trimethylsilylmethyl, the alkyl hydrazido(2−) product can be isolated, indicating that steric effects slow the migration. The resistence to migration in the iron(IV) compound in this case allowed us to characterize it in detail, and show that it has a high-spin ground state. The benzyl compound contrasts with the others, with a weak Fe–C bond leading to homolysis. DFT calculations support the feasibility of each proposed pathway and show that they are indeed expected to be kinetically competitive.

An important conclusion is that the use of formally iron(IV) centers enables migrations that can form N–C_{alkyl} as well as N–C_{aryl} bonds to a hydrazido(2−) ligand derived from N_2, showing the generalizability of this novel approach for forming N–C bonds that come from organometallic fragments and N_2. However, attempted migration of alkyl ligands is problematic when there is the potential to form a stabilized alkyl radical, because homolysis may result in rapid Fe–C bond cleavage. Thus, while alkyl migration was feasible for one case of N–C bond formation from N_2, the selectivity of the reaction was poorer for alkyl than the previously observed aryl migration.

Data availability

The data are in the ESI.†

Author contributions

S. F. M. and P. L. H. conceptualized the project, S. M. B. and R. X. H. and B. Q. M. collected and analyzed the data, S. M. B. wrote the original draft, and P. L. H. supervised the research and edited the manuscript.

Conflicts of interest

There are no conflicts to declare.

Acknowledgements

This research was solely supported by the U.S. Department of Energy, Office of Science, Office of Basic Energy Sciences, Catalysis Science program, under Award DE-SC0020315. We thank the Yale Center for Research Computing for guidance and use of the research computing infrastructure.

Notes and references

1 W. Nam, *Acc. Chem. Res.*, 2007, **40**, 522–531.
2 J. J. Scepaniak, C. G. Margarit, J. N. Harvey and J. M. Smith, *Inorg. Chem.*, 2011, **50**, 9508–9517.
3 J. M. Smith and D. Subedi, *Dalton Trans.*, 2012, **41**, 1423–1429.
4 S. A. Cramer, R. Hernández Sánchez, D. F. Brakhage and D. M. Jenkins, *Chem. Commun.*, 2014, **50**, 13967–13970.
5 W.-T. Lee, R. A. Juarez, J. J. Scepaniak, S. B. Muñoz, D. A. Dickie, H. Wang and J. M. Smith, *Inorg. Chem.*, 2014, **53**, 8425–8430.
6 S. B. Muñoz III, W.-T. Lee, D. A. Dickie, J. J. Scepaniak, D. Subedi, M. Pink, M. D. Johnson and J. M. Smith, *Angew. Chem., Int. Ed.*, 2015, **54**, 10600–10603.
7 A. K. Maity, J. Murillo, A. J. Metta-Magaña, B. Pinter and S. Fortier, *J. Am. Chem. Soc.*, 2017, **139**, 15691–15700.
8 I. S. Golovanov, A. V. Leonov, V. K. Lesnikov, E. V. Pospelov, K. V. Frolov, A. A. Korlyukov, Y. V. Nelyubina, V. V. Novikov and A. Y. Sukhorukov, *Dalton Trans.*, 2022, **51**, 4284–4296.
9 R. L. Lucas, D. R. Powell and A. S. Borovik, *J. Am. Chem. Soc.*, 2005, **127**, 11596–11597.
10 S. Kumar, A. S. Faponle, P. Barman, A. K. Vardhaman, C. V. Sastri, D. Kumar and S. P. de Visser, *J. Am. Chem. Soc.*, 2014, **136**, 17102–17115.
11 L. Wang, L. Hu, H. Zhang, H. Chen and L. Deng, *J. Am. Chem. Soc.*, 2015, **137**, 14196–14207.
12 B. Mondal, L. Roy, F. Neese and S. Ye, *Isr. J. Chem.*, 2016, **56**, 763–772.
13 J. L. Lee, D. L. Ross, S. K. Barman, J. W. Ziller and A. S. Borovik, *Inorg. Chem.*, 2021, **60**, 13759–13783.
14 D. Mansuy, J. P. Battioni, D. Dupre, E. Sartori and G. Chottard, *J. Am. Chem. Soc.*, 1982, **104**, 6159–6161.
15 A. Casitas, J. A. Rees, R. Goddard, E. Bill, S. DeBeer and A. Fürstner, *Angew. Chem., Int. Ed.*, 2017, **56**, 10108–10113.
16 B. P. Jacobs, P. T. Wolczanski, Q. Jiang, T. R. Cundari and S. N. MacMillan, *J. Am. Chem. Soc.*, 2017, **139**, 12145–12148.
17 K. P. Caulfield and Z. J. Tonzetich, *Organometallics*, 2022, **41**, 155–160.
18 B. K. Bower and H. G. Tennent, *J. Am. Chem. Soc.*, 1972, **94**, 2512–2514.

19 R. A. Lewis, D. E. Smiles, J. M. Darmon, S. C. E. Stieber, G. Wu and T. W. Hayton, *Inorg. Chem.*, 2013, **52**, 8218–8227.
20 Z. J. Tonzetich, F. Héroguel, L. H. Do and S. J. Lippard, *Inorg. Chem.*, 2011, **50**, 1570–1579.
21 I. M. Arafa, K. Shin and H. M. Goff, *J. Am. Chem. Soc.*, 1988, **110**, 5228–5229.
22 Z. Li and H. M. Goff, *Inorg. Chem.*, 1992, **31**, 1547–1548.
23 A. L. Balch, M. M. Olmstead, N. Safari and T. N. St. Claire, *Inorg. Chem.*, 1994, **33**, 2815–2822.
24 S. Byungho and H. M. Goff, *Inorg. Chim. Acta*, 1994, **226**, 231–235.
25 B. Song and H. M. Goff, *Inorg. Chem.*, 1994, **33**, 5979–5980.
26 C. G. Riordan and J. Halpern, *Inorg. Chim. Acta*, 1996, **243**, 19–24.
27 P. T. Matsunaga, C. R. Hess and G. L. Hillhouse, *J. Am. Chem. Soc.*, 1994, **116**, 3665–3666.
28 K. Koo and G. L. Hillhouse, *Organometallics*, 1996, **15**, 2669–2671.
29 X. Hu and K. Meyer, *J. Am. Chem. Soc.*, 2004, **126**, 16322–16323.
30 B. Chevrier, R. Weiss, M. Lange, J. C. Chottard and D. Mansuy, *J. Am. Chem. Soc.*, 1981, **103**, 2899–2901.
31 M. M. Olmstead, R. J. Cheng and A. L. Balch, *Inorg. Chem.*, 1982, **21**, 4143–4148.
32 I. Artaud, N. Gregoire, J. P. Battioni, D. Dupre and D. Mansuy, *J. Am. Chem. Soc.*, 1988, **110**, 8714–8716.
33 B. M. Hakey, D. C. Leary, J. C. Martinez, J. M. Darmon, N. G. Akhmedov, J. L. Petersen and C. Milsmann, *Organometallics*, 2022, **41**, 2268–2280.
34 S. F. McWilliams, D. L. J. Broere, C. J. V. Halliday, S. M. Bhutto, B. Q. Mercado and P. L. Holland, *Nature*, 2020, **584**, 221–226.
35 S. M. Bhutto, R. X. Hooper, B. Q. Mercado and P. L. Holland, *J. Am. Chem. Soc.*, 2023, **145**, 4626–4637.
36 S. M. Bhutto, B. Q. Mercado and P. L. Holland, *Inorg. Chem.*, 2023, **62**, 9335–9342.
37 A. L. Nagelski, M. S. Fataftah, M. M. Bollmeyer, S. F. McWilliams, S. N. MacMillan, B. Q. Mercado, K. M. Lancaster and P. L. Holland, *Chem. Sci.*, 2020, **11**, 12710–12720.
38 M. M. Deegan and J. C. Peters, *Chem. Sci.*, 2018, **9**, 6264–6270.
39 S. Bhutto, S. McWilliams, R. Hooper, B. Mercado and P. Holland, *ChemRxiv*, 2022, preprint, DOI: **10.26434/chemrxiv-2022-55shl**.
40 J. M. Smith, R. J. Lachicotte and P. L. Holland, *Organometallics*, 2002, **21**, 4808–4814.
41 J. Vela, S. Vaddadi, T. R. Cundari, J. M. Smith, E. A. Gregory, R. J. Lachicotte, C. J. Flaschenriem and P. L. Holland, *Organometallics*, 2004, **23**, 5226–5239.
42 T. J. J. Sciarone, A. Meetsma and B. Hessen, *Inorg. Chim. Acta*, 2006, **359**, 1815–1825.
43 K. C. MacLeod, I. M. DiMucci, E. P. Zovinka, S. F. McWilliams, B. Q. Mercado, K. M. Lancaster and P. L. Holland, *Organometallics*, 2019, **38**, 4224–4232.
44 M.-E. Moret and J. C. Peters, *J. Am. Chem. Soc.*, 2011, **133**, 18118–18121.
45 P. A. Rudd, N. Planas, E. Bill, L. Gagliardi and C. C. Lu, *Eur. J. Inorg. Chem.*, 2013, **2013**, 3898–3906.
46 S. F. McWilliams, E. Brennan-Wydra, K. C. MacLeod and P. L. Holland, *ACS Omega*, 2017, **2**, 2594–2606.
47 R. Hoffmann, S. Alvarez, C. Mealli, A. Falceto, T. J. Cahill, T. Zeng and G. Manca, *Chem. Rev.*, 2016, **116**, 8173–8192.
48 I. M. DiMucci, J. T. Lukens, S. Chatterjee, K. M. Carsch, C. J. Titus, S. J. Lee, D. Nordlund, T. A. Betley, S. N. MacMillan and K. M. Lancaster, *J. Am. Chem. Soc.*, 2019, **141**, 18508–18520.
49 A. D. Piascik, R. Li, H. J. Wilkinson, J. C. Green and A. E. Ashley, *J. Am. Chem. Soc.*, 2018, **140**, 10691–10694.
50 S. F. McWilliams, E. Bill, G. Lukat-Rodgers, K. R. Rodgers, B. Q. Mercado and P. L. Holland, *J. Am. Chem. Soc.*, 2018, **140**, 8586–8598.
51 K. P. Caulfield, J. Conradie, H. D. Arman, A. Ghosh and Z. J. Tonzetich, *Inorg. Chem.*, 2019, **58**, 15225–15235.
52 D. Kim, S. M. W. Rahaman, B. Q. Mercado, R. Poli and P. L. Holland, *J. Am. Chem. Soc.*, 2019, **141**, 7473–7485.
53 S. Barroso, A. M. Coelho, P. Adão, M. J. Calhorda and A. M. Martins, *Dalton Trans.*, 2017, **46**, 9692–9704.
54 H. Paulsen and A. X. Trautwein, in *Spin Crossover in Transition Metal Compounds III*, ed. P. Gütlich and H. A. Goodwin, Springer, Berlin, 2004, pp. 197–219.
55 R. E. Cowley, N. A. Eckert, J. Elhaïk and P. L. Holland, *Chem. Commun.*, 2009, 1760–1762.
56 N. A. Eckert, S. Vaddadi, S. Stoian, R. J. Lachicotte, T. R. Cundari and P. L. Holland, *Angew. Chem., Int. Ed.*, 2006, **45**, 6868–6871.
57 R. West, M. Ishikawa and R. E. Bailey, *J. Am. Chem. Soc.*, 1967, **89**, 4068–4072.
58 D. L. M. Suess and J. C. Peters, *J. Am. Chem. Soc.*, 2013, **135**, 4938–4941.
59 R. Poli, *C. R. Chim.*, 2021, **24**, 147–175.
60 G. S. Hammond, *J. Am. Chem. Soc.*, 1955, **77**, 334–338.